ACS Partner Journal

Journal of the American Society for Mass Spectrometry

pubs.acs.org/jasms

Research Article

Investigation of Product Ions Generated by 193 nm Ultraviolet Photodissociation of Peptides and Proteins Containing Disulfide Bonds

Luis A. Macias and Jennifer S. Brodbelt*

Cite This: *J. Am. Soc. Mass Spectrom.* 2022, 33, 1315−1324

Read Online

ACCESS | Metrics & More | Article Recommendations | Supporting Information

ABSTRACT: Disulfide bridges are unique post-translational modifications (PTM) that contribute to protein architecture and modulate function. This PTM, however, challenges top-down mass spectrometry by cyclizing stretches of the protein sequence. In order to produce and release detectable product ions that contribute to the assignment of proteoforms, regions of a protein encapsulated by disulfide bonds require two fragmentation events: cleavage of the protein backbone and cleavage of the disulfide bond. Traditional collisional activation methods do not cleave disulfide bonds efficiently, often leading to low sequence coverage of proteins that incorporate this feature. To address this challenge, we have evaluated the fragmentation pathways enabled by 193 nm ultraviolet photodissociation (UVPD) and UVPD coupled to electron transfer dissociation for the characterization of protein structures incorporating disulfide bonds. Cleavage of disulfide bonds by either approach results in S−S and C−S dissociation products that result from a combination of homolytic cleavage and hydrogen-transfer processes. Characterization of these product ions elevates interpretation of complex top-down spectra of proteins that incorporate disulfide bonds.

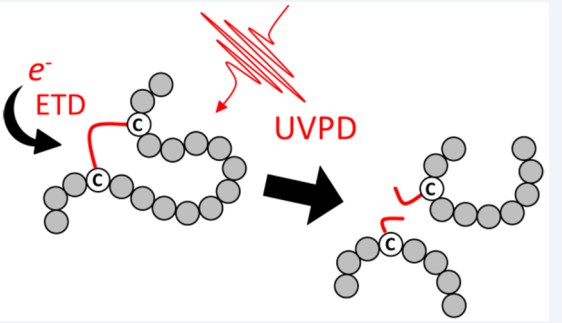

INTRODUCTION

Disulfide bridges are unique post-translational modifications (PTMs) that are integral to maintaining proper protein structure, folding, stability, and function.[1−3] Disulfide bridges cross-link cysteine residues to produce intraprotein sulfur−sulfur bonds between the amino acid side chains, imparting structural folds that maintain protein function, limit structural conformations, or prevent aggregation.[1−3] This prevalent modification naturally occurs across a wide range of protein classes, including kinases, neuropeptides, peptidic toxins, and antimicrobial peptides and is of particular interest for the development and synthesis of biotherapeutics, for which proper disulfide formation is essential.[2−5] While tandem mass spectrometry (MS/MS) is a powerful tool for the characterization of proteins and post-translational modifications, the presence of disulfide bridges creates special challenges. For traditional bottom-up mass spectrometry strategies in which proteins are enzymatically digested into smaller peptides prior to analysis, disulfide bonds are typically cleaved via chemical reduction and alkylation. The reduction/alkylation enhances the efficiency of proteolytic digestion but confounds the determination of locations and connectivities of the original disulfide bonds.

Top-down MS/MS is a powerful alternative approach for proteomic analyses, facilitating a more comprehensive view of protein sequence and modifications.[6−9] Top-down mass spectrometry directly interrogates intact protein sequences and is especially suited for the identification and characterization of distinct proteoforms.[6−9] The advantages of top-down proteomics, including the potential to pinpoint mutations, isoforms, and PTMs with single-residue resolution, depend on the ability to generate sufficiently high sequence coverage via cleavage of the peptide backbone during ion activation.[6−10] However, detection of diagnostic fragment ions produced from the backbone cleavages may be significantly hampered for protein structures that incorporate disulfide bridges, as this PTM cyclizes portions of the protein sequence that are flanked by the disulfide-linked cysteines. Generating sequence fragments within stretches containing disulfide bridges requires two fragmentation events, cleavage of peptide backbone and cleavage of the disulfide bond, to release detectable sequence fragments necessary for proteoform assignment, as illustrated in Scheme S1. In contrast to amide bonds, disulfide bonds do not readily dissociate upon traditional collisional activation, prohibiting characterization

Received: May 6, 2022
Revised: June 10, 2022
Accepted: June 13, 2022
Published: June 23, 2022

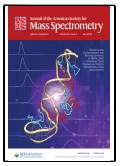

https://doi.org/10.1021/jasms.2c00124
J. Am. Soc. Mass Spectrom. 2022, 33, 1315−1324

of the cyclized portions of proteins.[10−13] Although chemical reduction of disulfide bonds followed by alkylation of the free thiols prior to analysis is commonly used to circumvent some of these challenges, chemical modification of thiols often precludes distinction of non-native disulfides, disrupts native-protein structure, and may complicate sample handling.[14−17] Furthermore, achieving only partial alkylation of thiols owing to inefficient reduction hinders release of sequence fragments and dilutes protein signal across multiple alkylation products in top-down workflows. Other strategies include electrochemical or photochemical derivatization to similarly disrupt disulfide bonds.[18−21]

Two promising yet not fully explored approaches that entirely sidestep lengthy or complicated derivatization strategies capitalize on alternative ion activation methods that cause direct cleavage of disulfide bonds in the gas phase and have shown potential for overcoming challenges encountered in top-down studies by this intractable PTM. In contrast to collision-based activation, cleavage of disulfide bonds is favorable in electron-based or photon-based activation methods. When subjected to electron capture (ECD) or electron transfer dissociation (ETD), protonated peptides become odd-electron radical species in which regardless of the electron-capture site radical migration to the disulfide bond and subsequent dissociation are highly favorable.[22−29] Moreover, concurrent irradiation of intact protein ions with infrared photons (IRMPD) during ETD, termed activated-ion ETD (AI-ETD),[30−32] dramatically enhances sequence coverage of proteins with intact disulfide bonds,[33] such as monoclonal antibodies,[34] over that achieved with collisional activation, ETD, or electron-transfer/higher-energy collision dissociation (EThcD).[35,36] Irradiation of ions with ultraviolet photons in a process termed ultraviolet photodissociation (UVPD)[10,37] also results in high sequence coverage and disulfide bond cleavage.[38−44] Utilizing 157 nm photons, both the S−S and amide bonds serve as a chromophores for photon absorption, leading to disulfide cleavage as well as peptide backbone dissociation.[39,40] Additionally, 266,[41] 213,[42,43] and 193 nm[44] UVPD have notable, yet distinct, uses for the characterization of disulfide bound peptides and proteins. While the absorption of 266 nm photons promoted exclusive cleavage of S−S bonds and allowed rapid elucidation of disulfide bond partners,[41] the absorption of 213 nm photons resulted in cleavage of the S−S bonds, C−S bonds, and amide bonds.[42,43] The latter method enabled the development of efficient search strategies that capitalized on the presence of diagnostic triplet fragment pairs and sequence fragments to simplify peptide assignments in bottom-up experiments.[42,43] 193 nm UVPD, in particular, has afforded near-complete sequence coverage for intact proteins while also inducing both peptide backbone and disulfide cleavages to untangle complex linkage patterns.[38,44] An innovative hybrid method integrating 266 nm UVPD, IRMPD, and ECD to characterize proteins with intact disulfide bonds demonstrated the value of combining ion activation methods to maximize coverage of protein sequences cyclized by disulfides.[45]

Despite the successful use of UVPD in the characterization of proteins with intact disulfide bonds, the detailed pathways for S−S and C−S bond dissociation and the resulting products have not been fully evaluated, especially for 193 nm UVPD. In contrast to electron-based activation for which radical migration and hydrogen rearrangements are known to induce R−S−S−R cleavage to result in R−S$^{\bullet}$ and R−SH products,[22,25−27] processes for UVPD are more complex and dependent on photon wavelength.[40−43] Although 266 nm UVPD is highly selective for homolytic cleavage of disulfides to exclusively yield R−S$^{\bullet}$ products,[41] 157 nm UVPD generates hydrogen rearrangement products, R−SH and R = S, in addition to homolytic cleavage R−S$^{\bullet}$-type products,[40] evincing the complexity of the products and pathways upon UVPD. Manifesting even higher complexity, 213 nm photoactivation causes cleavage of both C−S bonds and S−S bonds, introducing an additional channel through which disulfides may dissociate to release sequence fragments.[42,43] For 193 nm UVPD, neither the prevalence of homolytic versus hydrogen transfer products during S−S cleavage nor the formation of C−S cleavage products has been investigated in detail. Because losses and gains of hydrogen or sulfur atoms during hydrogen transfer and C−S cleavages mediate the resulting masses and m/z values of the products, accurately determining the predominant pathways is integral for confident fragment ion assignment. Careful examination of these phenomena stands to improve interpretation and fragment ion assignment of complex UVPD spectra and ultimately enhance MS/MS characterization of proteins that incorporate disulfide bonds. Here, 193 nm UVPD of model peptides was applied to elucidate distinct S−S and C−S cleavage products and define possible fragmentation pathways for disulfide dissociation. ETD-UVPD was investigated as a hybrid approach to modulate the favorability of specific disulfide cleavage pathways. As shown in this study, dissecting the UVPD and ETD-UVPD disulfide cleavage products aids spectral interpretation and boosts sequence coverage of intact proteins featuring disulfide bonds.

EXPERIMENTAL SECTION

Materials. Lysozyme, insulin, aprotinin, β-lactoglobulin, trypsin, formic acid, HPLC-grade water, and HPLC-grade acetonitrile (ACN) were acquired from Sigma-Aldrich (St. Louis, MO). Somatostatin was acquired from GenScript (Piscataway, NJ), and urotensin was procured from Cayman Chemical (Ann Arbor, MI). Peptide and protein digests were prepared by an overnight tryptic digestion at 37 °C. All samples were prepared in 50% ACN (v/v) with 0.1% formic acid at 5−10 μM concentration prior to mass spectrometry.

Mass Spectrometry. All mass spectra were collected on a Thermo Orbitrap Lumos mass spectrometer (San Jose, CA) equipped with a Coherent Excistar excimer laser (Santa Clara, CA) for 193 nm UVPD, as previously described.[46] Samples were infused via nanoelectrospray ionization (nESI) using gold/palladium-coated pulled-tip borosilicate glass capillaries and a Thermo Scientific Nanospray Flex ion source (San Jose, CA). Spray voltages were set to 1.0−2.0 kV. Spectra were collected at 120k resolution at m/z 200 at an AGC target of 1E5 to 5E5. For UVPD, precursor charge states were selected in the quadrupole with an appropriate isolation width (5−15 m/z) to capture the totality of the isotope distribution, prior to transfer to the dual linear ion trap for 193 nm UVPD. Product ions were subsequently transferred to the Orbitrap to collect MS/MS spectra. For ETD-UVPD, the selected precursor ion was initially subjected to electron-transfer reactions using fluoranthene as the electron-donating reagent anion. The charge-reduced precursor of charge $z-1$, where z is the initial precursor charge state, was subsequently reisolated prior to UVPD (MS^3). All UVPD was performed in the high-pressure

https://doi.org/10.1021/jasms.2c00124
J. Am. Soc. Mass Spectrom. 2022, 33, 1315−1324

linear ion trap. Three hundred microscans were averaged for UVPD and ETD-UVPD spectra.

Data Analysis. Data were processed using custom Python scripts by converting all spectra files into mzML formats to be read with the aid of the pyOpenMS Python package. Additional analyses were performed with the aid of Prosight Lite.

To discern relative abundances of product ions differing in mass by one hydrogen atom, theoretical isotope distributions were modeled using the chemical composition of product ions with the aid of pyOPenMS. The theoretical isotope distributions were fitted to the experimentally observed isotope distributions using a non-negative least-squares approach using the SciPy Python package. The fraction of each product ion contributing to the optimized fits was used as an indicator of the relative abundance of each product ion searched.

Top-down spectra for SOD were deconvoluted using the Xtract algorithm to produce a deisotoped mass list. The mass list was searched for *a, a+1, b, c, x, x+1, y, y−, y−2,* and *z* type fragment ions within a 10 ppm mass tolerance. Internal fragments were not considered in this search. For the search with "no modifications", any disulfide cleavage was considered as homolytic and thus resulted in no hydrogen transfer and no mass change. For searches considering heterolytic cleavages and C−S cleavages, respective mass differences were considered as variable modifications on cysteine residues with a maximum limit of 1 modification.

RESULTS AND DISCUSSION

193 nm UVPD S−S Cleavage Products. Production of sequence fragments from protein regions flanked by a disulfide depend on two cleavage events: peptide backbone cleavage and disulfide bond cleavage (Scheme S1). For 193 nm UVPD, peptide backbone dissociation is extensive, and frequently disulfide cleavage is sufficiently prevalent to allow the assignment of disulfide linkages.[37,38,44] However, the consequent S−S cleavage products have not yet been extensively characterized and may challenge spectral interpretation of top-down spectra for proteins with intact disulfide bonds. Specifically, products may originate from homolytic S−S cleavage without or with hydrogen transfer (Scheme 1A), and assignment of these products is instrumental for accurate interpretation of fragment ions and curation of MS/MS spectra. Previous studies utilizing 266 nm UVPD-MS noted the exclusive production of homolytic cleavage products,[41] contrasting with 157 nm UVPD-MS for which both homolytic and hydrogen transfer products were observed.[40] Although 193 nm UVPD is known to cleave disulfide bonds,[44] the factors governing the pathways have not yet been evaluated.

Scheme 1. Summary of S−S and C−S Cleavage Products Observed via 193 nm UVPD

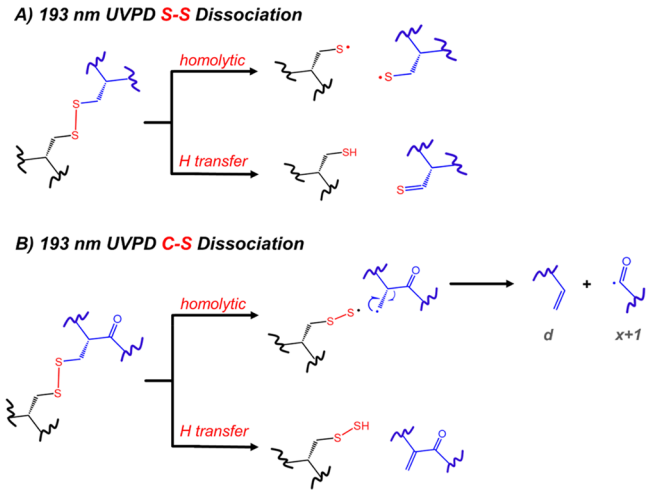

To determine the predominance of the possible S−S cleavage products for 193 nm UVPD, peptide pairs cross-linked by a single disulfide bond were produced and subjected to UVPD to induce disulfide cleavage and release peptide products. The resulting masses of the free peptides inform the abundance of disulfide cleavage occurring homolytically versus with hydrogen transfer (as defined in Scheme 1). For example, somatostatin contains one disulfide bond. Tryptic digestion of somatostatin cleaves the Lys-Thr peptide bond and generates a peptide pair composed of AGCKNFFWK (chain A) and TFTSC (chain B), covalently linked by a single disulfide (Figure 1A) and shifting the net mass of the peptide by 18.01 Da owing to peptide bond hydrolysis.[47] Upon 193 nm UVPD of the disulfide-bound peptide pair (2+), the resulting MS/MS spectrum was searched for products arising from homolytic disulfide cleavage as well as satellite hydrogen transfer product ions corresponding to a gain or loss of one hydrogen atom, labeled +1H and −1H, relative to the homolytic cleavage product, the latter labeled 0H (Figure 1B). For the disulfide-linked somatostatin peptide, complementary single-charged product ions corresponding to disulfide cleavage are observed: m/z 1099.52 (chain A) and m/z 557.22 (chain B). Hydrogen transfer (−1H and +1H) products for are also observed: m/z 1098.52 (−1H) and 1100.53 (+1H) for chain A and m/z 556.21 (−1H) and 558.22 (+1H) for chain B (Figure 1C). The presence of these trios of fragment ions (−1H, 0H, +1H) confirms that multiple pathways are involved in S−S cleavage during UVPD. The observed intensity of each ion is not directly informative of the relative abundance of the assigned product owing to interference of overlapping isotopic isomers. Explicitly, the first and second ^{13}C isotopologues of the −1H product are isobaric with the 0H and +1H products and contribute to the total ion abundances. Similarly, the ^{13}C isotopologue of the 0H product overlaps with the +1H product. Extracting relative abundances of homolytic disulfide cleavage products versus those that incorporate hydrogen transfer thus requires examining the entire isotopic distribution of the peptide products.

To uncover the relative contributions of the −1H, 0H, and +1H products to the isotopic distribution of the disulfide-cleaved peptide products, a non-negative least-squares approach was implemented to fit a theoretical mixture of all product isotope distributions to the observed distribution, as described in the Experimental Section. Percentages of each product contributing to the optimized theoretical fit are indicative of the relative product abundance (−1H, 0H, +1H products) and are summarized as donut plots in Figure 2 adjacent to the histograms of the experimental isotopic distributions and modeled fits. As demonstrated in Figure 2A for chain A generated upon UVPD of somatostatin, the observed distribution shown in the donut plot is primarily composed of the −1H product (65.8%), followed by the +1H product (32.3%), and a minor abundance of the 0H product (1.9%). Complementary products were observed for somatostatin chain B where the +1H product (83.1%) was predominant with a lower abundance of the −1H (16.3%)

https://doi.org/10.1021/jasms.2c00124
J. Am. Soc. Mass Spectrom. 2022, 33, 1315−1324

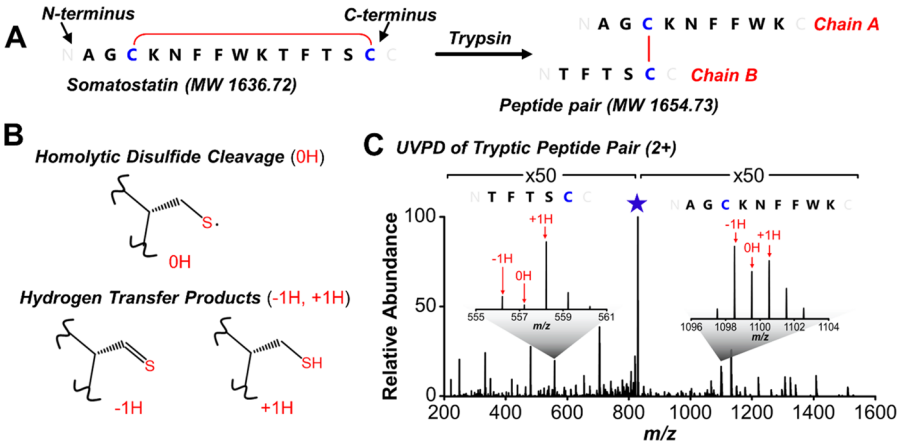

Figure 1. (A) Tryptic digestion of somatostatin results in a disulfide-bound peptide pair composed of two chains, chain A (AGCKNFFWK) linked to chain B (TFTSC), via tryptic cleavage of the K−T bond. (Note that there was no evidence of production of peptide pair corresponding to tryptic cleavage of K−N, resulting in AGCK linked to NFFWKTFTSC.) (B) UVPD causes homolytic disulfide cleavage, labeled 0H, which may occur with hydrogen transfer, labeled −1H and +1H. (C) 193 nm UVPD of the tryptic peptide pair product of somatostatin (2+) induces cleavage of the disulfide bond to yield a mixture of homolytic disulfide cleavage and hydrogen transfer products. Insets display expansions of the disulfide-cleaved product ions. The precursor ion is labeled with a star.

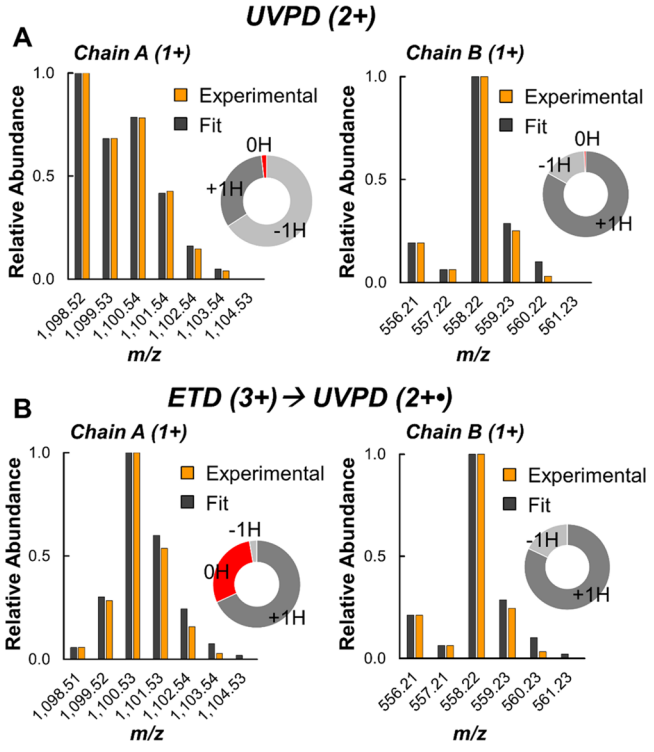

Figure 2. Isotope distributions produced for chain A and chain B free peptide products via (A) UVPD and (B) ETD-UVPD of digested somatostatin were modeled as a mix of products originating from homolytic dissociation of disulfide bonds (0H) and disulfide cleavage with hydrogen transfer (−1H, +1H). Abundances of each product ion used to construct each fit are shown as donut plot insets.

and 0H (0.6%) products (Figure 2A). Altogether, these results indicate that S−S cleavage occurs almost exclusively via hydrogen transfer for UVPD of digested somatostatin, favoring H abstraction from chain A onto chain B. The accuracy of the non-negative least-squares approach to determine the relative abundance of these product ions was assessed by applying the same analysis to the digested-somatostatin precursor ions (Figure S1). For the precursor ions, the isotope distribution should be attributed solely to the 0H form and no −1H or +1H species should be detected, as no gains or losses of hydrogen are expected for the intact molecular ion. Accordingly, the modeled fit for the precursor ions should be 0% −1H, 100% 0H, and 0% −1H, while deviations from this distribution are attributed to error. For the 2+ precursor (Figure S1A), the fitted distribution was composed of 97.5% ± 0.03% for 0H as well as 2.5% ± 0.03% for 1H and 0.0 ± 0% for +1H (n = 3), indicating high reproducibility with a low error of <3% and only a slight overestimation of −1H species. These low errors were also produced for the 3+ precursor (1.6 ± 0.1% for −1H, 98.4 ± 0.1% for 0H, 0.0 ± 0.0% for +1H, n = 3) and 4+ precursor (2.7 ± 0.3% for −1H, 97.3 ± 0.3% for 0H, 0.0 ± 0.0% for +1H, n = 3) in Figure S1B,C. These results suggest that the non-negative least-squares approach is adequate for modeling isotopic distributions with moderate accuracy.

Interestingly, the degree of hydrogen transfer is notably dependent on the charge states of both the precursor and product ions, in which a higher charge state of the precursor ion favors homolytic disulfide cleavage without hydrogen transfer. UVPD of digested-somatostatin in the 2+, 3+, and 4+ charge states produced both the chain A and the chain B products suitable for isotopic analysis (Figure S2). Figure S3 summarizes the relative contributions of the −1H, 0H, and +1H products to the observed isotope distribution of chain A for each precursor charge state, showing the significant increase in the portion of homolytic S−S cleavage (0H) relative to hydrogen transfer products (−1H, + 1H) as the precursor charge state of somatostatin increases. Examination of the results for chain B reveals the same trend (Figure S4). Among the collection of UVPD spectra shown for somatostatin in Figure S2, the chain A product was detected in three different charge states (1+, 2+, 3+). The portion of the 0H product for chain A increases with its charge state (Figure S3). Moreover, while hydrogen-transfer products are dominant for the lowest product and precursor ion charge states, the 0H products are favored for the highest charge states. Ultimately, these findings demonstrate that homolytic cleavage of S−S bonds is possible during UVPD and may occur in conjunction with hydrogen

https://doi.org/10.1021/jasms.2c00124
J. Am. Soc. Mass Spectrom. 2022, 33, 1315−1324

transfer in a manner that is influenced by both precursor and product ion charge states.

A second peptide, urotensin II, was examined to generalize the trends. Upon tryptic digestion, this 12-residue peptide produces AGTADCFWK (chain A) linked to YCV (chain B) by a single disulfide bond, and UVPD releases the two chains (Figure S5). Only −1H and +1H products were observed for Chain B, but all three products (−1H, 0H, +1H) were observed for Chain A upon UVPD of each of the urotensin precursor charge states (1+, 2+, 3+) (Figure S6). The abundance of the 0H product for Chain A did not show the same charge-dependent trend noted above for digested-somatostatin, suggesting that hydrogen-transfer processes likely depend on additional sequence-specific factors. Three additional disulfide-linked peptide pairs (named L1, L2, L3) were produced from a tryptic digest of lysozyme (Figure S7), characterized by UVPD (Figure S8), and subjected to the same isotopic analysis of free peptide products, as summarized in in Table S1. Again, these peptides presented variable abundances of the −1H, 0H, and +1H products, further establishing that S−S bond cleavage during 193 nm UVPD is a prevalent process and may occur with hydrogen transfer mediated by multiple factors, including charge state and peptide sequence.

Increasing S−S Cleavage Efficiency via ETD-UVPD. Electron-based dissociation methods favor disulfide cleavage and have been incorporated into hybrid MS/MS methods to enhance performance metrics of collisional activated dissociation and photodissociation strategies.[33,34,45] For example, integrating ECD with 266 nm UVPD on an FTICR platform improved the characterization of intact proteins containing disulfide bonds, suggesting that combining activation methods enhanced S−S cleavage.[45] To explore the merits of hybrid electron/photon dissociation in the present study using an Orbitrap platform, a hybrid ETD-UVPD approach was implemented to allow comparison of the fragment ion distributions from disulfide-linked peptides using ETD, UVPD, or ETD-UVPD. For the hybrid approach ETD-UVPD, a disulfide-linked peptide was selected for ETD to produce an odd-electron charge-reduced precursor ion, which was subsequently isolated and subjected to 193 nm UVPD. Spectra for this MS^3 method are displayed in Figure S9 for the 3+ charge state of digested-somatostatin, which was first activated by ETD to produce the charge reduced 2+• ETnoD product (Figure S9A). The charge-reduced product was then isolated and subjected to 193 nm UVPD (Figure S9B), resulting in dominant release of the two chains from the disulfide-linked peptide. ETD and ETD-UVPD mass spectra for 2+ and 4+ charge states for the same somatostatin peptide are shown in Figures S10 and S11.

To compare the three methods, the abundances of the free A and B chains as a percentage of the total ion current (TIC) were calculated for ETD, UVPD, and ETD-UVPD of 2+, 3+, and 4+ charge states of digested somatostatin (Figure S12). The total portion of the peptide chain products was typically less than 1% for ETD, except for the 4+ precursor where the chain A was 4.5% (1+) and 11.6% (2+) of the TIC. Electron-based methods are highly charge dependent and often perform best for peptide ions with high charge densities, as evidenced by the high S−S cleavage propensity observed for the somatostatin precursor in the highest charge state (4+). Following ETD by a stage of UVPD to activate the charge-reduced ETnoD precursors (2+ → 1+•, 3+ → 2+•, and 4+ → 3+•) resulted in variable abundances of the A and B chains that tended to be greatest for lower precursor charge states (Figure S12C). For example, the chain A product (1+) constituted 19.8% of the TIC for ETD-UVPD of the 2+ precursor (2+ → 1+•), or 12.4% (2+ product) or 0.7% (1+ product) for ETD-UVPD of the 3+ precursor (3+ → 2+•). However, for the highest charge state of somatostatin, ETD-UVPD (4+ → 3+•) resulted in lower abundances of the free peptide chains (2.3% for chain A (2+) and 0.3% for chain B (1+)).

For UVPD versus ETD-UVPD, the free peptide chains produced upon S−S cleavage were typically less than 1% abundance by UVPD alone (Figure S12B) and were significantly enhanced by employing ETD-UVPD (Figure S12C). For example, 193 nm UVPD of digested-somatostatin (2+) resulted in 0.2%, 0.05%, and 0.2% of the ion current for chain A (1+), chain A (2+), and chain B (1+) ions, respectively, and UVPD of the 3+ charge state yielded similarly low abundances of the free chains (0.01%, 1.0%, and 0.2% TIC for chain A (1+), chain A (2+), and chain B (1+), respectively). ETD-UVPD (3+ → 2+•) resulted in greater chain A abundances: 12.4% (1+) and 0.7% (2+) of the TIC and even higher chain A abundance (19.8%) for the 2+ somatostatin precursor (2+ → 1+•). The performance attributes of hybrid ETD-UVPD were further evaluated by analysis of additional disulfide-linked peptide pairs (urotensin and three disulfide-bound tryptic peptides from lysozyme) as illustrated in Figures S13−S16 and summarized in Table S2. ETD-UVPD consistently resulted in greater abundances of S−S cleavage products, mirroring results achieved for digested-somatostatin. The significant increases in S−S cleavage efficiency for hybrid ETD-UVPD relative to UVPD or ETD alone underscores the benefits of utilizing 193 nm UVPD to enhance ETD analyses.

As described previously for UVPD, the isotope distributions of the free peptide chains generated by ETD-UVPD upon S−S cleavage were examined in detail for somatostatin (Figure 2B). In addition to −1H, 0H, and +1H products, isotope distribution models also considered the possibility of +2H products to account for additional hydrogen migration known to occur during electron activation methods. Modeling isotope distributions for singly charged chain B and chain A products from digested-somatostatin (3+ → 2+•) produced by ETD-UVPD (Figure 2B) shows that while the isotope distribution of chain B products is similar to the one obtained by UVPD (Figure 2A), the distribution of chain A products features a significant decrease in −1H abundance concomitant with increase in 0H and +1H species. The change for chain A is attributed to preferential electron capture occurring on the larger chain to favor more hydrogen-rich fragments while the smaller chain B remains unperturbed by the electron capture process. This outcome is repeated for ETD-UVPD of additional charge states of digested-somatostatin (Figure S17), where chain B featured a mix of −1H, 0H, and +1H products while chain A displayed strong propensity toward 0H and +1H products. Additionally, the +2H product was observed for chain A (2+) from ETD-UVPD of the somatostatin peptide in the 4+ charge state (4+ → 3+•), implying electron capture at chain A along with additional hydrogen migration. Isotope distributions for ETD-UVPD of digested urotensin yielded similar results where chain B reflected the type of isotope distributions observed upon UVPD alone (dominant −1H and +1H products), while the larger chain A favored 0H and +1H products as well as a + 2H

https://doi.org/10.1021/jasms.2c00124
J. Am. Soc. Mass Spectrom. 2022, 33, 1315−1324

product observed only for ETD-UVPD of triply charged urotensin (3+ → 2+•) (Figure S18). Similarly for lysozyme peptide pairs, preferential formation of 0H and +1H products was observed for ETD-UVPD (Table S3), notably contrasting the much greater amount of −1H products generated by UVPD.

Cleavage of Multiple Disulfides via UVPD and ETD-UVPD. Because proteins may incorporate multiple disulfide bonds, multiple S−S cleavage events might be required to produce fragment ions by MS/MS. In this context, the capabilities of and products resulting from UVPD and ETD-UVPD were evaluated by analysis of insulin. Insulin is a protein composed of two peptide chains (shorter chain A and longer chain B) linked by two interpeptide disulfide bonds (Figure S19A), both of which must be cleaved to release the two chains. UVPD and ETD-UVPD spectra acquired for multiple charge states of insulin (4+, 5+, 6+) were searched for chain A and B ions as −2H, −1H, 0H, +1H, and +2H products, accounting for all combinations of hydrogen transfers and homolytic cleavages of both disulfide bonds. For each charge state, both UVPD and ETD-UVPD resulted in cleavage of both interpeptide S−S bonds to release both the A and B chains (Figure S19), as noted in the past.[44] The abundances of the free chains were generally greater for ETD-UVPD compared to UVPD (Figure S20), analogous to the findings for the somatostatin and urotensin peptide pairs linked by a single disulfide bond. Isotope distributions were examined in detail for UVPD of 4+ and 5+ precursor ions and the charge-reduced 4+• and 5+• ions (from ETnoD) to determine the relative abundances of −2H, −1H, 0H, +1H, +2H, and +3H products. For the 4+ and 4+• precursors, chain A (1+) predominantly displayed the 0H product with minor abundances of all the other products (Figure S21A). For the B chain (3+), a shift was observed to favor more hydrogen-rich products, especially +1H and +2H products, for the odd-electron precursor (4+•), whereas the distribution for the even-electron precursor (4+) was centered at 0H. Analogous results were produced for 5+ and 5+• insulin precursors, for which product distributions were centered at 0H for chain A products (1+ and 2+) for both UVPD and ETD-UVPD, whereas there was again a notable shift toward higher H content (+1H, + 2H) for the chain B products (3+ and 4+) upon ETD-UVPD (Figure S21B). The significant increase in H content for chain B is likely due its larger size, enhancing the potential for hydrogen migration during separation of the A and B chains. Overall, these results illustrate the complexity of hydrogen transfer occurring upon UVPD and ETD-UVPD for proteins incorporating multiple disulfide bonds.

Impact of S−S Cleavage on Sequence Ions from UVPD and ETD-UVPD. As described above, dissociation of S−S bonds by UVPD (or ETD-UVPD) occurs in conjunction with hydrogen-transfer processes to release free peptide chains. The hydrogen transfer mass shifts may also be propagated in the sequence fragments that originate from the cleaved peptide chains. For example, producing the a_6 ion from chain A (AGCKNFFWK) of digested-somatostatin requires concomitant cleavage of the disulfide bond and cleavage of the Phe-Phe C_α-C bond, while generating the y_4 ion does not require disulfide cleavage and is not expected to incur hydrogen transfer (Figure S22A). Isotope distributions for these sequence fragments can be searched with gains or losses of hydrogen atoms, as shown for a_6 and y_4 in Figure S22. Comparing hydrogen content between sequence fragments that necessitate S−S cleavage, categorized as "SS-cleaved", to the hydrogen content of sequence fragments that do not, classified as "free" fragments, will be important for customizing accurate search algorithms for proper identification of fragment ions.

Hydrogen content of sequence fragments produced from digested somatostatin, digested urotensin, and insulin via UVPD and ETD-UVPD was monitored and used to calculate a weighted average hydrogen content value for each sequence ion by scaling the relative contributions of +1H/−1H/0H products to the overall isotope distribution. A positive number for the weighted average hydrogen content favors +1H products, and a negative number favors −1H products. For example, a_6 and y_4 presented weighted average hydrogen contents of 0.55 and −0.05, respectively, by UVPD, and weighted average hydrogen contents of 0.76 and −0.06 by ETD-UVPD. The near-zero values for the y_4 ions are consistent with the expectation of a standard backbone cleavage process without hydrogen migration. The significantly higher values for the a_6 ions reflect a much greater involvement of hydrogen transfer, attributed to the evolution of these fragment ions from disulfide cleavage. These values were calculated for sequence fragments (listed in Table S4) detected in UVPD (total of 463 ions examined) and ETD-UVPD (263 ions examined) mass spectra of digested somatostatin, digested urotensin, and insulin to construct histograms tracking the frequency of each value for SS-cleaved and free fragment ions (Figure 3). Free sequence fragments generated by UVPD predominantly displayed a unimodal distribution centered near 0H (Figure 3A), indicating a low preponderance of hydrogen-shifted fragments when disulfide cleavage is not necessary for fragment production. In contrast, the SS-cleaved fragments display a multimodal distribution with one of the distributions centered at near 0H, indicating no hydrogen shifts, and a second distribution spanning +0.5H to +1.0H, as well as a third minor distribution emerging near −1.0H. These results underscore that sequence ions generated by UVPD that require disulfide cleavage are significantly influenced by hydrogen-transfer processes akin to the production of the chain A and B species from disulfide cleavage alone.

Similar results were observed for the fragment ions created by ETD-UVPD (Figure 3C). The contrast between free fragments and SS-cleaved fragments is again readily apparent. Free fragments displayed a predominant distribution near 0H, indication of little involvement of hydrogen transfer, and with smaller populations clustering around −1H and +0.75H. The major distribution of the SS-cleaved fragment ions spanned 0.5H to 1.0 H (centered at 0.80H). Utilizing UVPD to dissociate ETnoD products results in significant shifts in hydrogen content, disfavoring a weighted content of 0H to instead promote formation of product ions with a weighted hydrogen content of +1H. This effect is attributed to the hydrogen-rich ETnoD precursor resulting in aberrant hydrogen content. The broader and more heterogeneous distributions observed for the ETD-UVPD fragment ions versus those for UVPD reflect the additional tendency of electron activation to promote hydrogen-transfer processes.[22,26,27]

Cleavage of C−S Bonds. 213 nm UVPD of peptides containing disulfide bonds is reported to cause dissociation of C−S bonds, providing an additional avenue through which disulfides may be cleaved to release fragments.[42] Accordingly, UVPD and ETD-UVPD spectra acquired using 193 nm photons were searched for C−S cleavage products. For

https://doi.org/10.1021/jasms.2c00124
J. Am. Soc. Mass Spectrom. 2022, 33, 1315−1324

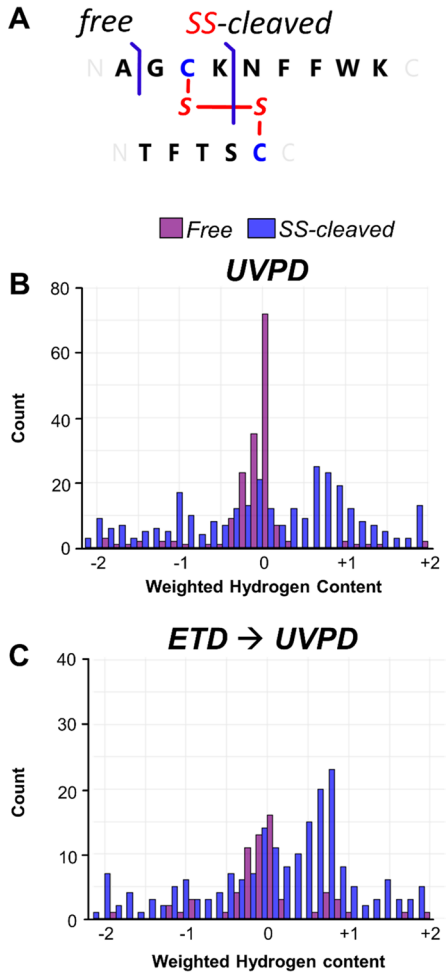

Figure 3. (A) Fragment ions produced from insulin, digested somatostatin, and digested urotensin were classified as "free" or "SS cleaved", depending on whether cleavage of a disulfide bond is necessary for detection of the product. The weighted hydrogen content was calculated for each product ion generated via (B) UVPD (463 ions) or (C) ETD-UVPD (263 ions) and plotted in respective histograms for each activation method. Lists of fragment ions are included in Table S4.

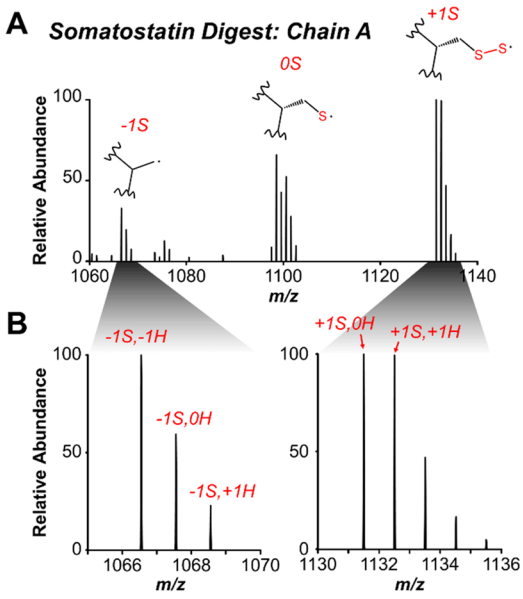

Figure 4. (A) 193 nm UVPD of the digested somatostatin (2+) results in cleavage of C−S bonds, confirmed by the presence of the free peptide fragment of chain A with the gain and loss of a sulfur atom. (B) Sulfur-rich and -deficient products both yield fragments with masses indicative of homolytic cleavage of C−S (0H) and hydrogen transfer events (+1H, −1H). The full UVPD spectrum is shown in Figure 1C.

digested-somatostatin, C−S dissociation would release the peptide chains with either a gain or loss of a sulfur atom. For the 2+ charge state precursor ion of somatostatin, C−S cleavage product ions of m/z 1067.55 and 1131.50 were observed for chain A, corresponding to the loss (−1S) and gain (+1S) of sulfur, respectively (Figure 4). Furthermore, masses corresponding to concurrent gains and losses of hydrogen during C−S dissociation were also observed, suggesting a mixture of fragmentation pathways as was demonstrated for S−S dissociation. Inspection of the isotope distributions of the −1S and +1S Chain A products in conjunction with possible hydrogen transfer processes (−1H, 0H, +1H) revealed that the −1S product was exclusively detected with hydrogen loss (−1S/−1H), whereas the +1S product was detected without hydrogen transfer (+1S/0H) or with hydrogen transfer (+1S/+1H), as shown in Figure S23A. Upon UVPD of chain B (1+), C−S cleavage products of m/z 525.24 and 589.19 were generated, corresponding to −1S/−1H and both +1S/0H and +1S/+1H ions (Figure S24) based on careful analysis of the isotope distributions (Figure S23B). Interestingly, while the +1S/0H products imply homolytic cleavage of the C−S bond without hydrogen transfer, the complementary fragment, −1S/0H, was not detected for either chain A or B. For 213 nm UVPD, it has been reported that when homolytic C−S cleavage occurs, the sulfur-deficient (−1S) product may decompose into a *d* and *x+1* fragment at the position of the cysteine, as illustrated in Figure S23A.[42] For chain A, the x_6/x_6+1 fragments were detected at m/z 895.44/896.45, and for chain B, the d_5 fragment was detected at m/z 480.25, confirming that any −1S/0H products possibly formed during homolytic cleavage of C−S likely decompose into *x+1* and *d* fragments (Figure S25). Considering the hydrogen transfer products +1S/+1H and −1S/−1H observed for both peptide chains, these fragments are complementary and suggest that during hydrogen transfer the sulfur-rich peptide abstracts a hydrogen from the sulfur-deficient peptide chain during their separation after C−S cleavage.

These results were corroborated by examination of UVPD spectra of different charge states of disulfide-linked peptide-pairs from digested somatostatin (Figure S26A), digested urotensin (Figure S26B), and digested lysozyme (Tables S5 and S6), all revealing a predominance of −1S/−1H, +1S/0H, +1S/+1H products. Although −1S/0H fragments were observed in some cases, this does not contradict the proposed fragmentation trends but rather confirms that homolytic cleavage of C−S may occur without hydrogen transfer to generate +1S/0H and −1S/0H products, ions that readily decompose into secondary fragments (such as *d/x+1*). C−S cleavage was also observed upon ETD-UVPD, as demonstrated for digested somatostatin in Figures S27−S29. Generally, similar trends were observed upon ETD-UVPD of the same peptide pairs (Figure S30 and Tables S7 and S8), favoring −1S/−H, +1S/0H, +1S/+H, with only occasional exceptions, such as the significant presence of +1S/+2H for certain peptides in specific charge states.

https://doi.org/10.1021/jasms.2c00124
J. Am. Soc. Mass Spectrom. 2022, 33, 1315−1324

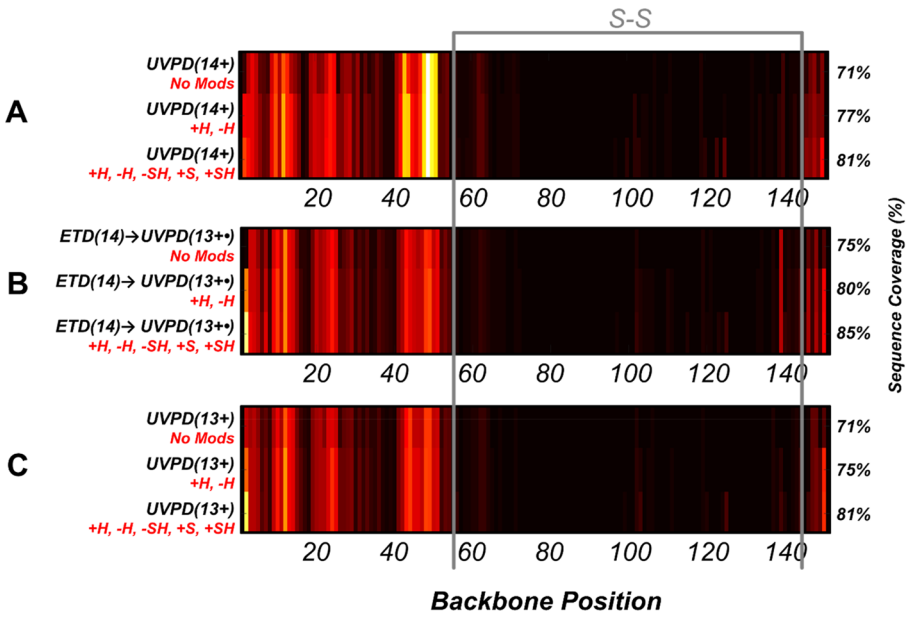

Figure 5. Heatmap of backbone cleavage sites (sum of *a, a+1, b, c, x, x+1, y, y−1, y−2,* and *z* type fragments originating from cleavage at each backbone position, <10 ppm error) that result in detectable fragment ions from superoxide dismutase (denatured) produced by (A) UVPD (14+), (B) ETD-UVPD (14+), and (C) UVPD (13+). Fragment ions were searched assuming all S−S cleavage events are due to homolytic cleavage (No Mods) and by including variable modifications due to hydrogen transfer (+H, −H) and variable modifications due to C−S cleavage (+H, −H, −SH, +S, +SH). The location of the disulfide bond is indicated by the gray bracket. Backbone cleavages spanning positions 60−140 are observed in low abundance, and more detailed lists of fragment ions are included in Table S9.

193 nm UVPD and ETD-UVPD of Proteins Containing Disulfide Bonds. The findings above illustrating the prevalence of hydrogen-transfer pathways that accompany scission of disulfide bonds motivated our interest in exploring the fragmentation of intact proteins containing disulfide bonds. Considering all prominent pathways for disulfide cleavage via 193 nm UVPD, sequence ions generated from protein regions containing disulfide bonds may be produced directly from homolytic cleavage of S−S bonds or with the following modifications: +H, −H, −SH, +S, and +SH. A comprehensive search of top-down UVPD mass spectra for all of these product types should boost sequence coverage of disulfide-bound regions. To explore this effect, superoxide dismutase (SOD), a protein incorporating a single disulfide bond, was subjected to UVPD. Upon ESI, the prominent 14+ charge state was isolated and subjected to UVPD (1 pulse; 3 mJ/pulse) (Figure S31, Table S9). Searching for standard UVPD fragments (*a, a+1, b, c, x, x+1, y, y−1, y−2, z*) resulted in 71% sequence coverage (Figure 5A), assuming no disulfide-related fragment modifications (i.e., exclusively homolytic cleavage of S−S bonds without hydrogen transfer). Notably, coverage of the disulfide-bound region was sparse, and only a few low abundance fragment ions were identified. Including potential products from disulfide cleavage with hydrogen transfer (+H and − H) via searching with a variable modification on the cysteine residues (the two participating in the disulfide bond) resulted in a slight increase in sequence coverage to 77%. Expanding the search to include C−S cleavage products (−SH, +S, and +SH) boosted sequence coverage to 81%. In sum, searching for all possible disulfide cleavage modifications (−H, +H, −SH, +S, +SH) resulted in a 10% increase in sequence coverage for top-down analysis of SOD. The search results for UVPD of a second charge state, 13+, mirror the same trend observed for the 14+ charge state (Figure 5C).

To compare the performance of ETD-UVPD for the same protein, the 14+ charge state of SOD was isolated and subjected to ETD to generate the charge-reduced 13+• ion which was isolated and subjected to 193 nm UVPD. The resulting ETD-UVPD spectrum was searched for sequence fragments with no modifications to yield a coverage of 75% (Figure 5B), providing a slight increase over the 71% coverage achieved by UVPD alone. Searching for +H and −H variable modifications on the disulfide-bound cysteines yielded a coverage of 80%, while expanding the search to include all possible modifications (−H, +H, −SH, +S, +SH) resulted in a coverage of 85%, amounting to an overall 10% increase in sequence coverage over a more standard top-down search that does not incorporate the additional product ions.

Although sequence coverage for SOD benefitted from utilizing ETD-UVPD relative to UVPD alone, this effect is not universal and largely depends on the protein identity. For example, in the case of *β*-lactoglobulin (an 18.3 kDa protein containing 2 disulfides), ETD-UVPD resulted in a significant drop in sequence coverage relative to UVPD alone, even when sequence fragments were searched with variable modifications (Figure S32). For aprotinin, a small 6.5 kDa protein featuring 3 disulfide bonds, although ETD-UVPD resulted in a lower sequence coverage (46%) compared to UVPD (54%), the fragments observed by ETD-UVPD were complementary to those observed with only UVPD. Combining fragment identifications from both approaches results in a sequence coverage of 70% or a 16% increase compared to UVPD alone, as shown on the respective fragment maps (Figure S33). Additionally, it should also be noted that the presence and search for fragment ions offset by 1 Da can introduce ambiguity into fragment assignment. The deconvolution of top-down spectra may result in 1 Da mass shifts that are not due to specific hydrogen-transfer events. Additionally, searching for additional fragments incorporating 1 Da mass

https://doi.org/10.1021/jasms.2c00124
J. Am. Soc. Mass Spectrom. 2022, 33, 1315−1324

shift will inevitably increase the total number of fragment assignments and concurrently also increase the number of false assignments. Addressing these potential concerns will require a greater understanding of fragmentation pathways to accurately distinguish mass shifts related to disulfide cleavages from other artifacts as well as development of methods to control false discovery rates for fragment ions in top-down spectra.

CONCLUSIONS

As evidenced from the results presented in this study and summarized in Scheme 1, 193 nm UVPD cleaves both S−S bonds and C−S bonds homolytically or in conjunction with hydrogen transfer to generate products of variable hydrogen content. For S−S cleavage, all product ion types are prevalent upon UVPD, whereas ETD-UVPD results in even more abundant products and slightly favors those entailing hydrogen transfer. For C−S cleavage, the ion retaining the additional sulfur was frequently observed as a stable product, whereas the fragment losing the sulfur atom commonly decomposed into *d* and *x* products, as also noted previously for 213 nm UVPD. When C−S cleavage occurred in conjunction with hydrogen transfer, the chain retaining the additional sulfur atom abstracted a hydrogen atom from the chain losing the sulfur atom, generating complementary +1S/+1H and −1S/−1H in a manner also mirrored for ETD-UVPD. The results showcased in this study also illustrate that there are some potential benefits to combining electron and photon-based activation techniques to boost characterization of proteins which exhibit patchy coverage in regions spanned by the disulfide bonds. A promising approach would be to explore ETUVPD[48] or ECuvPD,[49] in which both activation techniques occur concurrently and avoid excluding a significant portion of the ion current that occurs during the second isolation step in an MS^3 strategy. Such an approach may be more apt to capitalize on the complementarity of electron and photon-based ion activation techniques to interrogate proteins containing disulfide bonds.

ASSOCIATED CONTENT

Supporting Information

The Supporting Information is available free of charge at https://pubs.acs.org/doi/10.1021/jasms.2c00124.

Lists of fragments used to construct Figure 3 (Table S4) (XLSX)

Supplemental spectra, bar graphs, and tables depicting fragment abundances (PDF)

Lists of fragments used to construct Figure 5 (Table S9) (XLSX)

AUTHOR INFORMATION

Corresponding Author

Jennifer S. Brodbelt − *Department of Chemistry, University of Texas at Austin, Austin, Texas 78712, United States;* orcid.org/0000-0003-3207-0217; Email: jbrodbelt@cm.utexas.edu

Author

Luis A. Macias − *Department of Chemistry, University of Texas at Austin, Austin, Texas 78712, United States;* orcid.org/0000-0003-1949-6029

Complete contact information is available at: https://pubs.acs.org/10.1021/jasms.2c00124

Notes

The authors declare no competing financial interest.

ACKNOWLEDGMENTS

Funding from NSF (CHE-2203602), the Robert A. Welch Foundation (F-1155), and the UT System for support of the UT System Proteomics Core Facility Network is gratefully acknowledged. Research reported in this publication was supported by the National Cancer Institute of the National Institutes of Health under Award No. F31CA257404 to L.A.M. The content is solely the responsibility of the authors and does not necessarily represent the official views of the National Institutes of Health.

REFERENCES

(1) Fass, D. Disulfide Bonding in Protein Biophysics. *Annual Review of Biophysics* **2012**, *41*, 63−79.

(2) Feige, M. J.; Braakman, I.; Hendershot, L. M. Disulfide Bonds in Protein Folding and Stability. *Oxidative Folding of Proteins: Basic Principles, Cellular Regulation and Engineering*; Wiley, 2018; Chapter 1.1, pp 1−33.

(3) Wiedemann, C.; Kumar, A.; Lang, A.; Ohlenschläger, O. Cysteines and Disulfide Bonds as Structure-Forming Units: Insights From Different Domains of Life and the Potential for Characterization by NMR. *Frontiers in Chemistry* **2020**, DOI: 10.3389/fchem.2020.00280.

(4) Xu, D.; Lu, W. Defensins: A Double-Edged Sword in Host Immunity. *Frontiers in Immunology* **2020**, DOI: 10.3389/fimmu.2020.00764.

(5) Liu, H.; May, K. Disulfide Bond Structures of IgG Molecules. *mAbs* **2012**, *4*, 17−23.

(6) Chen, B.; Brown, K. A.; Lin, Z.; Ge, Y. Top-Down Proteomics: Ready for Prime Time? *Anal. Chem.* **2018**, *90*, 110−127.

(7) Catherman, A. D.; Skinner, O. S.; Kelleher, N. L. Top Down Proteomics: Facts and Perspectives. *Biochem. Biophys. Res. Commun.* **2014**, *445*, 683−693.

(8) Toby, T. K.; Fornelli, L.; Kelleher, N. L. Progress in Top-Down Proteomics and the Analysis of Proteoforms. *Annual Review of Analytical Chemistry* **2016**, *9*, 499−519.

(9) Melby, J. A.; Roberts, D. S.; Larson, E. J.; Brown, K. A.; Bayne, E. F.; Jin, S.; Ge, Y. Novel Strategies to Address the Challenges in Top-Down Proteomics. *J. Am. Soc. Mass Spectrom.* **2021**, *32*, 1278−1294.

(10) Macias, L. A.; Santos, I. C.; Brodbelt, J. S. Ion Activation Methods for Peptides and Proteins. *Anal. Chem.* **2020**, *92*, 227−251.

(11) Mitchell Wells, J.; McLuckey, S. A. Collision-Induced Dissociation (CID) of Peptides and Proteins. In *Methods in Enzymology*; Biological Mass Spectrometry; Academic Press, 2005; Vol. *402*, pp 148−185.

(12) Lioe, H.; OrsHair, R. A. J. A Novel Salt Bridge Mechanism Highlights the Need for Nonmobile Proton Conditions to Promote Disulfide Bond Cleavage in Protonated Peptides under Low-Energy Collisional Activation. *J. Am. Soc. Mass Spectrom.* **2007**, *18*, 1109−1123.

(13) Mentinova, M.; Han, H.; McLuckey, S. A. Dissociation of Disulfide-Intact Somatostatin Ions: The Roles of Ion Type and Dissociation Method. *Rapid Commun. Mass Spectrom.* **2009**, *23*, 2647−2655.

(14) Wiesner, J.; Resemann, A.; Evans, C.; Suckau, D.; Jabs, W. Advanced Mass Spectrometry Workflows for Analyzing Disulfide Bonds in Biologics. *Expert Rev Proteomics* **2015**, *12*, 115−123.

(15) Foley, S. F.; Sun, Y.; Zheng, T. S.; Wen, D. Picomole-Level Mapping of Protein Disulfides by Mass Spectrometry Following Partial Reduction and Alkylation. *Anal. Biochem.* **2008**, *377*, 95−104.

(16) Albert, A.; Eksteen, J. J.; Isaksson, J.; Sengee, M.; Hansen, T.; Vasskog, T. General Approach To Determine Disulfide Connectivity in Cysteine-Rich Peptides by Sequential Alkylation on Solid Phase and Mass Spectrometry. *Anal. Chem.* **2016**, *88*, 9539−9546.

(17) Lakbub, J. C.; Shipman, J. T.; Desaire, H. Recent Mass Spectrometry-Based Techniques and Considerations for Disulfide Bond Characterization in Proteins. *Anal Bioanal Chem.* **2018**, *410*, 2467−2484.
(18) Cramer, C. N.; Haselmann, K. F.; Olsen, J. V.; Nielsen, P. K. Disulfide Linkage Characterization of Disulfide Bond-Containing Proteins and Peptides by Reducing Electrochemistry and Mass Spectrometry. *Anal. Chem.* **2016**, *88*, 1585−1592.
(19) Cui, L.; Ma, Y.; Li, M.; Wei, Z.; Fei, Q.; Huan, Y.; Li, H.; Zheng, L. Disulfide Linkage Assignment Based on Reducing Electrochemistry and Mass Spectrometry Using a Lead Electrode. *Talanta* **2019**, *199*, 643−651.
(20) Yang, X.; Xia, Y. Mapping Complex Disulfide Bonds via Implementing Photochemical Reduction Online with Liquid Chromatography-Mass Spectrometry. *J. Am. Soc. Mass Spectrom.* **2021**, *32*, 307−314.
(21) Yang, X.; Zhang, L.; Xia, Y. Photochemical Disulfide-Ene Modification Enhances Protein Sequencing and Disulfide Mapping by Mass Spectrometry. *Anal. Chem.* **2021**, *93*, 15231−15235.
(22) Zubarev, R. A.; Kruger, N. A.; Fridriksson, E. K.; Lewis, M. A.; Horn, D. M.; Carpenter, B. K.; McLafferty, F. W. Electron Capture Dissociation of Gaseous Multiply-Charged Proteins Is Favored at Disulfide Bonds and Other Sites of High Hydrogen Atom Affinity. *J. Am. Chem. Soc.* **1999**, *121*, 2857−2862.
(23) Fort, K. L.; Cramer, C. N.; Voinov, V. G.; Vasil'ev, Y. V.; Lopez, N. I.; Beckman, J. S.; Heck, A. J. R. Exploring ECD on a Benchtop Q Exactive Orbitrap Mass Spectrometer. *J. Proteome Res.* **2018**, *17*, 926−933.
(24) Riley, N. M.; Coon, J. J. The Role of Electron Transfer Dissociation in Modern Proteomics. *Anal. Chem.* **2018**, *90*, 40−64.
(25) Zubarev, R. A.; Horn, D. M.; Fridriksson, E. K.; Kelleher, N. L.; Kruger, N. A.; Lewis, M. A.; Carpenter, B. K.; McLafferty, F. W. Electron Capture Dissociation for Structural Characterization of Multiply Charged Protein Cations. *Anal. Chem.* **2000**, *72*, 563−573.
(26) Tan, L.; Durand, K. L.; Ma, X.; Xia, Y. Radical Cascades in Electron Transfer Dissociation (ETD) - Implications for Characterizing Peptide Disulfide Regio-Isomers. *Analyst* **2013**, *138*, 6759−6765.
(27) Cole, S. R.; Ma, X.; Zhang, X.; Xia, Y. Electron Transfer Dissociation (ETD) of Peptides Containing Intrachain Disulfide Bonds. *J. Am. Soc. Mass Spectrom.* **2012**, *23*, 310−320.
(28) Lermyte, F.; Sobott, F. Electron Transfer Dissociation Provides Higher-Order Structural Information of Native and Partially Unfolded Protein Complexes. *PROTEOMICS* **2015**, *15*, 2813−2822.
(29) Zhang, J.; Ogorzalek Loo, R. R.; Loo, J. A. Increasing Fragmentation of Disulfide-Bonded Proteins for Top-Down Mass Spectrometry by Supercharging. *Int. J. Mass Spectrom.* **2015**, *377*, 546−556.
(30) Riley, N. M.; Westphall, M. S.; Hebert, A. S.; Coon, J. J. Implementation of Activated Ion Electron Transfer Dissociation on a Quadrupole-Orbitrap-Linear Ion Trap Hybrid Mass Spectrometer. *Anal. Chem.* **2017**, *89*, 6358−6366.
(31) Riley, N. M.; Westphall, M. S.; Coon, J. J. Activated Ion-Electron Transfer Dissociation Enables Comprehensive Top-Down Protein Fragmentation. *J. Proteome Res.* **2017**, *16*, 2653−2659.
(32) Riley, N. M.; Sikora, J. W.; Seckler, H. S.; Greer, J. B.; Fellers, R. T.; LeDuc, R. D.; Westphall, M. S.; Thomas, P. M.; Kelleher, N. L.; Coon, J. J. The Value of Activated Ion Electron Transfer Dissociation for High-Throughput Top-Down Characterization of Intact Proteins. *Anal. Chem.* **2018**, *90*, 8553−8560.
(33) Rush, M. J. P.; Riley, N. M.; Westphall, M. S.; Coon, J. J. Top-Down Characterization of Proteins with Intact Disulfide Bonds Using Activated-Ion Electron Transfer Dissociation. *Anal. Chem.* **2018**, *90*, 8946−8953.
(34) Lodge, J. M.; Schauer, K. L.; Brademan, D. R.; Riley, N. M.; Shishkova, E.; Westphall, M. S.; Coon, J. J. Top-Down Characterization of an Intact Monoclonal Antibody Using Activated Ion Electron Transfer Dissociation. *Anal. Chem.* **2020**, *92*, 10246−10251.
(35) Swaney, D. L.; McAlister, G. C.; Wirtala, M.; Schwartz, J. C.; Syka, J. E. P.; Coon, J. J. Supplemental Activation Method for High-Efficiency Electron-Transfer Dissociation of Doubly Protonated Peptide Precursors. *Anal. Chem.* **2007**, *79*, 477−485.
(36) Frese, C. K.; Altelaar, A. F. M.; van den Toorn, H.; Nolting, D.; Griep-Raming, J.; Heck, A. J. R.; Mohammed, S. Toward Full Peptide Sequence Coverage by Dual Fragmentation Combining Electron-Transfer and Higher-Energy Collision Dissociation Tandem Mass Spectrometry. *Anal. Chem.* **2012**, *84*, 9668−9673.
(37) Brodbelt, J. S.; Morrison, L. J.; Santos, I. Ultraviolet Photodissociation Mass Spectrometry for Analysis of Biological Molecules. *Chem. Rev.* **2020**, *120*, 3328−3380.
(38) Shaw, J. B.; Li, W.; Holden, D. D.; Zhang, Y.; Griep-Raming, J.; Fellers, R. T.; Early, B. P.; Thomas, P. M.; Kelleher, N. L.; Brodbelt, J. S. Complete Protein Characterization Using Top-Down Mass Spectrometry and Ultraviolet Photodissociation. *J. Am. Chem. Soc.* **2013**, *135*, 12646−12651.
(39) Shaw, J. B.; Liu, W.; Vasil'ev, Y. V.; Bracken, C. C.; Malhan, N.; Guthals, A.; Beckman, J. S.; Voinov, V. G. Direct Determination of Antibody Chain Pairing by Top-down and Middle-down Mass Spectrometry Using Electron Capture Dissociation and Ultraviolet Photodissociation. *Anal. Chem.* **2020**, *92*, 766−773.
(40) Fung, Y. M. E.; Kjeldsen, F.; Silivra, O. A.; Chan, T. W. D.; Zubarev, R. A. Facile Disulfide Bond Cleavage in Gaseous Peptide and Protein Cations by Ultraviolet Photodissociation at 157 Nm. *Angew. Chem.* **2005**, *117*, 6557−6561.
(41) Agarwal, A.; Diedrich, J. K.; Julian, R. R. Direct Elucidation of Disulfide Bond Partners Using Ultraviolet Photodissociation Mass Spectrometry. *Anal. Chem.* **2011**, *83*, 6455−6458.
(42) Talbert, L. E.; Julian, R. R. Directed-Backbone Dissociation Following Bond-Specific Carbon-Sulfur UVPD at 213 Nm. *J. Am. Soc. Mass Spectrom.* **2018**, *29*, 1760−1767.
(43) Bonner, J.; Talbert, L. E.; Akkawi, N.; Julian, R. R. Simplified Identification of Disulfide, Trisulfide, and Thioether Pairs with 213 Nm UVPD. *Analyst* **2018**, *143*, 5176−5184.
(44) Quick, M. M.; Crittenden, C. M.; Rosenberg, J. A.; Brodbelt, J. S. Characterization of Disulfide Linkages in Proteins by 193 Nm Ultraviolet Photodissociation (UVPD) Mass Spectrometry. *Anal. Chem.* **2018**, *90*, 8523−8530.
(45) Wongkongkathep, P.; Li, H.; Zhang, X.; Ogorzalek Loo, R. R.; Julian, R. R.; Loo, J. A. Enhancing Protein Disulfide Bond Cleavage by UV Excitation and Electron Capture Dissociation for Top-down Mass Spectrometry. *Int. J. Mass Spectrom.* **2015**, *390*, 137−145.
(46) Klein, D. R.; Holden, D. D.; Brodbelt, J. S. Shotgun Analysis of Rough-Type Lipopolysaccharides Using Ultraviolet Photodissociation Mass Spectrometry. *Anal. Chem.* **2016**, *88*, 1044−1051.
(47) Chrisman, P. A.; McLuckey, S. A. Dissociations of Disulfide-Linked Gaseous Polypeptide/Protein Anions: Ion Chemistry with Implications for Protein Identification and Characterization. *J. Proteome Res.* **2002**, *1*, 549−557.
(48) Cannon, J. R.; Holden, D. D.; Brodbelt, J. S. Hybridizing Ultraviolet Photodissociation with Electron Transfer Dissociation for Intact Protein Characterization. *Anal. Chem.* **2014**, *86*, 10970−10977.
(49) Shaw, J. B.; Malhan, N.; Vasil'ev, Y. V.; Lopez, N. I.; Makarov, A.; Beckman, J. S.; Voinov, V. G. Sequencing Grade Tandem Mass Spectrometry for Top-Down Proteomics Using Hybrid Electron Capture Dissociation Methods in a Benchtop Orbitrap Mass Spectrometer. *Anal. Chem.* **2018**, *90*, 10819−10827.

https://doi.org/10.1021/jasms.2c00124
J. Am. Soc. Mass Spectrom. 2022, 33, 1315−1324